JCIM JOURNAL OF CHEMICAL INFORMATION AND MODELING

Article

Cite This: J. Chem. Inf. Model. 2019, 59, 2190−2198

pubs.acs.org/jcim

Free Energies of Catalytic Species Adsorbed to Pt(111) Surfaces under Liquid Solvent Calculated Using Classical and Quantum Approaches

Xiaohong Zhang, Ryan S. DeFever, Sapna Sarupria, and Rachel B. Getman*

Department of Chemical and Biomolecular Engineering, Clemson University, Clemson, South Carolina 29634-0909, United States

Supporting Information

ABSTRACT: Solvent plays an important role in liquid phase heterogeneous catalysis; however, methods for calculating the free energies of catalytic phenomena at the solid−liquid interface are not well-established. For example, solvent molecules alter the energies of catalytic species and participate in catalytic reactions and can thus significantly influence catalytic performance. In this work, we begin to establish methods for calculating the free energies of such phenomena, specifically, by employing an explicit solvation method using a multiscale sampling (MSS) approach. This MSS approach combines classical molecular dynamics with density functional theory. We use it to calculate the free energies of solvation of catalytic species, specifically adsorbed NH*, NH_2*, CO*, COH*, CH_2OH*, and $C_3H_7O_3$* on Pt(111) surfaces under aqueous phase and under a mixed H_2O/CH_3OH solvent. We compare our calculated values with analogous values from implicit solvation for validation and to identify situations where implicit solvation is sufficient versus where explicit solvent is needed to compute adsorbate free energies. Our results indicate that explicit quantum-based methods are needed when adsorbates form chemical bonds and/or strong hydrogen bonds with H_2O solvent. Using MSS, we further separate the calculated free energies into energetic and entropic contributions in order to understand how each influences the free energy. We find that adsorbates that exhibit strong energies also exhibit strong and negative entropies, and we attribute this relationship to hydrogen bonding between the adsorbates and the solvent molecules, which provides a large energetic contribution but reduces the overall mobility of the solvent.

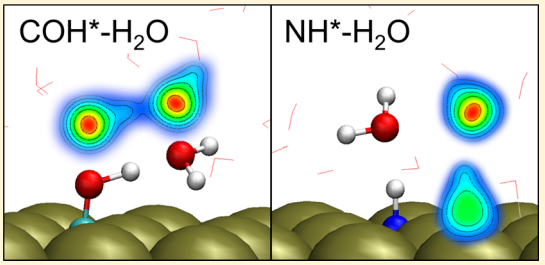

1. INTRODUCTION

Calculating the free energies of catalytic adsorbates under liquid phase is imperative for modeling catalyst performance in liquid phase reaction conditions; however, methods for performing such calculations remain unresolved. In general, the *energies* of catalytic species must be calculated with quantum mechanics (QM), which captures the potential energies that are stored within the chemical bonds. The *free energies* are influenced by the thermal movements of the atoms and molecules (including the solvent molecules) and thus require finite-temperature methods. Present strategies for calculating free energies of catalytic adsorbates in liquid reaction conditions entail summing the adsorbate's free energy calculated under vacuum (F_{ads}^{vac}) with its free energy of solvation (ΔF_{sol}),[1−11] i.e.

$$F_{ads}^{liq}(T) = F_{ads}^{vac}(T) + \Delta F_{sol}(T) \quad (1)$$

where $F_{sol}(T)$ is the difference in free energy between a solvated adsorbate and the same adsorbate under vacuum at temperature T, and $F_{ads}^{vac}(T)$ is the free energy of the adsorbate under vacuum at temperature T calculated relative to the energy of the adsorbate at 0 K,[12−18] i.e.

$$F_{ads}^{vac}(T) = E_{elec}^{vac} + E_{ZP}^{vac} + \Delta F_{vib}^{vac}(T) \quad (2)$$

Here, E_{elec}^{vac} and E_{ZP}^{vac} are the electronic and zero-point vibrational energies calculated with QM (at 0 K), and $\Delta F_{vib}^{vac}(T)$ is its temperature-dependent vibrational free energy calculated relative to E_{ZP}^{vac}. $\Delta F_{sol}(T)$ is most often calculated in quantum mechanics using implicit solvation,[1,3−6,8−10,19] which collapses the thermal effects of the solvent into a continuum based on the solvent's dielectric constant. This method thus does not include solvent molecules explicitly. Save for one comparison of this strategy with an analogous method employing explicit solvation (calculated using a combination of QM and molecular mechanics, i.e., QM/MM) for calculating the free energy of a single reaction (i.e., $(CHOH)_2$* → 2CHOH*, where * are catalyst sites) on a Pt(111) catalyst,[7] the validity and limitations of using implicit solvation for calculating free energies involved in heterogeneous liquid phase catalysis remain to be established. In situations where solvent molecules interact strongly with catalytic adsorbates and/or participate in the catalytic reaction, it is expected that implicit solvation will be insufficient.

Special Issue: Women in Computational Chemistry

Received: January 29, 2019
Published: March 1, 2019

DOI: 10.1021/acs.jcim.9b00089
J. Chem. Inf. Model. 2019, 59, 2190−2198

For the purposes of this study, we focus on H_2O solvent. H_2O molecules are known to form hydrogen bonds with adsorbates, which influence the adsorbates' energies significantly.[6−10,20−27] In some cases, these hydrogen bonds seem to have specific interactions with catalytic adsorbates, for example, discriminating between different conformers of the same adsorbate and even altering the relative stabilities of these conformers compared to gas phase.[21,22,24,25] It is unclear that implicit solvation has the precision to capture such phenomena. When solvent molecules participate in catalytic chemistry, the limitations of implicit solvation are more pronounced. For example, H_2O molecules have been shown to participate in aqueous phase heterogeneously catalyzed reactions by helping to promote bond breaking and forming processes.[20,22,26,28−31] Modeling such phenomena requires including at least one H_2O molecule explicitly in the simulation; yet, there is no well-established method for calculating free energies for adsorbates on heterogeneous catalyst surfaces using explicit solvation. It is thus important to establish methods for broadly calculating the free energies of catalytic adsorbates in liquid reaction conditions.

It is our goal in this work to begin establishing such methods, as well as to provide guidelines for when implicit solvation can and cannot be employed for calculating the free energies of catalytic phenomena in liquid reaction conditions. Specifically, we employ a multiscale sampling (MSS) approach[27,31−33] that combines density functional theory (DFT) with classical molecular dynamics (MD) for calculating the free energies of solvation of catalytic adsorbates under explicit solvation. In this method, MD is used to generate configurations of liquid solvent molecules, and DFT is used to calculate their energies. This method thus takes advantage of the strengths of both DFT—accurately calculating system energies—and MD—efficiently producing configurations of liquid solvent molecules at finite T. We use this method to calculate the free energies of solvation of NH*, NH_2*, CO*, COH*, CH_2OH*, and $C_3H_7O_3$* adsorbates on Pt(111) catalysts under liquid solvent. We are interested in these adsorbates because they are important in ammonia synthesis and biomass processing, which are reactions of societal interest,[34,35] and because they demonstrate different interactions with the solvent environment. In order to establish guidelines for when implicit solvation can be used for calculating free energies and when explicit solvation is needed, we compare free energies of solvation calculated with explicit solvation using MSS for these adsorbates to implicit solvation. We find that the COH*, CH_2OH*, and $C_3H_7O_3$* adsorbates, which comprise −OH groups that form strong hydrogen bonds with H_2O, require explicit solvation to fully capture solvation energies; however, implicit solvation is sufficient for the remaining adsorbates considered in this work. Using the MSS approach, we are additionally able to parse the calculated free energies of solvation into energetic and entropic contributions, which enables analysis of the origins of these contributions. We find that adsorbates that interact strongly with H_2O also exhibit large and negative entropies of solvation, which are caused by decreased rotational dynamics of H_2O molecules that are strongly bonded to the adsorbates.

2. COMPUTATIONAL METHODS

2.1. System Setup. Pt catalysts are modeled with periodic, three-layer 3 × 3 Pt(111) slabs in monoclinic supercells ($\alpha = \beta = 90°$, $\gamma = 60°$) constructed from the structure of bulk Pt. The structure of bulk Pt is face centered cubic with a lattice parameter of 3.967 Å and interatomic Pt−Pt distances of 2.805 Å. There is one adsorbate per slab, giving a total adsorbate coverage of 1/9 monolayer (ML, where 1 ML is equal to 1 adsorbate per surface metal atom). The arrangements of adsorbates on the surfaces are configured such that the distances between neighboring adsorbates are maximized. Positions of the adsorbates on the surface are selected according to the literature.[27,36,37] Adsorbate conformations are obtained by performing geometry relaxations using DFT as described in Section 2.4. The volume of the simulation boxes above the Pt surfaces are initially set such that the H_2O density is ∼1 g/cm^3, and these box dimensions are refined according to the particular adsorbate as follows. The procedure is described in detail in a concurrent publication[32] and illustrated schematically in Figure S2 in the Supporting Information. First, 54 H_2O molecules are randomly placed above the top surfaces of the Pt slabs. Positions of the H_2O molecules are refined by performing energy minimizations with the Large-scale Atomic/Molecular Massively Parallel Simulator (LAMMPS,[38] details about the simulations are provided in Section 2.2) using the conjugate gradient method until the relative change in energy between successive iterations ($\Delta E/E$) falls below 10^{-8} and the maximum force on any atom falls below 10^{-10} kcal/mol-Å. Following energy minimization, the system is equilibrated via a 2 ns MD simulation performed in the canonical (NVT) ensemble, where the temperature is maintained at 300 K using the thermostat of Bussi et al.[39] This simulation is followed by a 500 ps simulation performed in the microcanonical (NVE) ensemble to check for energy conservation. Finally, an MD simulation is performed in the isothermal−isobaric (NPT) ensemble to determine the appropriate height of the simulation box. The NPT simulation is carried out for a total of 5 ns at 300 K and 1 atm, maintained by the Nosé−Hoover thermostat and barostat[40,41] along with a temperature damping parameter of 100 fs and a stressing damping parameter of 5 ps. The resulting average simulation box heights vary from 35 to 38 Å, depending on the adsorbate. The average water density in the bulk regions of the simulation boxes (i.e., the regions where the water densities as functions of distance from the Pt surfaces have plateaued) is 1.01 ± 0.01 g/cm^3, which compares favorably with the reported value of 1.002 g/cm^3 at 1 bar and 298 K for the water model employed in this work (TIP3P/CHARMM;[42,43] see Section 2.2 for more details). After the simulation box heights have been determined, configurations of liquid solvent molecules are generated in MD using the canonical (NVT) ensemble. These simulations are carried out at 300 K for a total of 5 ns, where the first 2 ns are used for system equilibration and the remaining 3 ns are used to sample configurations of H_2O molecules. When the configurations from MD are used for DFT calculations, an additional 14 Å of vacuum space is added above the top of the H_2O layer, resulting in box heights of 49 to 52 Å. The reason for this is to minimize the dipole interactions between neighboring cells in the c direction in the DFT calculations. Since there is minimal (if any) perturbation to the H_2O structure in DFT calculations (see Section 2.4), changes in the local H_2O densities around the adsorbate due to this change are negligible. We performed several test calculations to determine the influence of the simulation box size on quantities of interest for this Article, and they are discussed in the Supporting Information.

DOI: 10.1021/acs.jcim.9b00089
J. Chem. Inf. Model. 2019, 59, 2190−2198

For comparison, we also calculate the thermodynamics of solvation of catalytic adsorbates in a 50%/50% by weight solution of H_2O and CH_3OH. These systems utilize the same 3 × 3 Pt(111) slabs and contain 27 H_2O molecules and 15 CH_3OH molecules. Otherwise, the systems are set up analogously to the pure H_2O systems.

2.2. Classical MD Simulations. Energies in LAMMPS are calculated classically. H_2O and CH_3OH solvent molecules are allowed to be flexible and are modeled with the TIP3P/CHARMM[42,44] and OPLS-AA[45] force fields, respectively. All other species are held rigid. Intermolecular energies are calculated using pairwise Lennard-Jones + Coulomb (LJ + C) potentials. LJ parameters for the Pt atoms are taken from the universal force field (UFF),[46] and LJ parameters for surface adsorbates are taken from the OPLS-AA force field. All LJ cross terms are calculated with geometric mixing rules, except for the intermolecular O−H interactions between H_2O molecules, which use Lorentz−Berthelot mixing rules.[47,48] Coulomb terms for Pt atoms and surface adsorbates are their calculated partial charges, which are obtained from charge densities calculated in DFT. These are used instead of the Coulomb terms defined by the UFF and OPLS-AA force fields to capture the charge redistribution that occurs between the adsorbates and the Pt surface atoms upon adsorption. Partial charges are calculated using the Density Derived Electrostatic and Chemical (DDEC) method.[49] Further details about charge partitioning calculations are provided in the Supporting Information. The cutoff value for LJ + C interactions is 7 Å. Long-ranged Coulomb interactions are calculated using the Particle−Particle Particle−Mesh (PPPM) method[50] with the accuracy set to 10^{-4}. All LJ and C parameters, as well as intramolecular parameters for H_2O and CH_3OH solvent molecules are provided in the Supporting Information. As the MD simulations are used to generate configurations of solvent molecules and the DFT results depend on the configurations that are generated, the DFT results depend on the classical potentials and other decisions employed in the MD simulations. We investigated the effects of different potentials for H_2O and Pt on the number of solvent molecules that hydrogen bond with the adsorbates studied in this work. We found minor to modest differences. These tests are discussed further in the Supporting Information.

2.3. Free Energies. Solvation free energies of the adsorbates presented in this work are calculated in two ways: with multiscale sampling using a combination of DFT and MD (ΔF_{sol}^{MSS}) and with implicit solvation using DFT (ΔF_{sol}^{imp}).

2.3.1. Multiscale Sampling. Values of ΔF_{sol}^{MSS} combine energies calculated with DFT with entropies calculated with MD, i.e.

$$\Delta F_{sol}^{MSS} = \Delta E_{int}^{DFT} - T\Delta S_{int}^{MD} \quad (3)$$

where ΔE_{int}^{DFT} is the adsorbate−water interaction energy calculated with DFT, T is the temperature, and ΔS_{int}^{MD} is the adsorbate−water interaction entropy calculated with MD. More details about the derivation of this equation are provided in the Supporting Information. Since one cannot directly output entropies from an MD simulation, we extract entropies from MD-calculated free energies (ΔF_{sol}^{MD}, see eq 6). These are calculated using the method of thermodynamic integration. In this method, a solute (here, the Pt surface with adsorbate) is "grown" in a sea of solvent over the course of an MD simulation performed in the NVT ensemble. This growth is simulated by scaling the LJ and C parameters between the solute and solvent via scaling parameters, λ_{LJ} and λ_C, respectively. These scaling parameters take on values from 0 (LJ or C cross terms are equal to 0) to 1 (LJ or C cross terms are equal to their normal values). In order to avoid singularities when $\lambda_{LJ} = 0$, a soft core potential implemented in LAMMPS is used.[51] The free energy is

$$\Delta F_{Pt+ads}^{MD} = \int_{\lambda=0}^{\lambda=1} \left\langle \frac{\partial \Delta E(\lambda)}{\partial \lambda} \right\rangle_{\lambda} d\lambda \quad (4)$$

where E is the energy of interaction between the Pt surface + adsorbate with the solvent molecules at different values of λ, where λ can be either λ_{LJ} or λ_C (these are varied one at a time, following the method outlined by Shirts and Pande[51]). Values of $\langle \partial \Delta E(\lambda)/\partial \lambda \rangle_{\lambda}$ are obtained by making small perturbations to λ ($\delta\lambda = 0.0001$) and calculating the differences in E. Herein, we use 21 equally spaced values of λ ($\lambda = 0, 0.05, 0.10, ..., 1$) to evaluate ΔF^{MD}. For each value of λ, a NVT MD simulation is performed for 350 ps, where the first 100 ps are used for system equilibration and the last 250 ps are used for configurational sampling. Further details about the influence of the length of the NVT trajectory on the results are provided in the Supporting Information. Configurations are sampled every 1 ps over the production run of the NVT MD trajectory in order to calculate E. Since this yields the free energy of solvation for the Pt + adsorbate system, we additionally calculate ΔF^{MD} for the clean Pt surface, which allows us to separate the contribution due to the adsorbate.

$$\Delta F_{sol}^{MD} = \Delta F_{Pt+ads}^{MD} - \Delta F_{Pt}^{MD} \quad (5)$$

ΔS_{int}^{MD} is obtained by decomposing ΔF_{sol}^{MD} into energetic and entropic contributions[52,53]

$$\Delta S_{int}^{MD} = \frac{\Delta F_{sol}^{MD} - \Delta E_{int}^{MD}}{T} \quad (6)$$

where ΔE_{int}^{MD} is calculated by simply evaluating the LJ + C potential between the solvent molecules and the adsorbate at various configurations of solvent molecules over the course of a straightforward (i.e., without the scaling parameter λ) NVT MD trajectory.

ΔE_{int}^{DFT} (used in eq 3 to calculate ΔF_{sol}^{MSS}) comprises all of the physical and chemical interactions between the liquid solvent molecules and the adsorbate and is calculated as

$$\Delta E_{int}^{DFT} = \langle (E_{Pt+ads}^{liq} - E_{Pt+ads}^{vac}) - (E_{Pt}^{liq} - E_{Pt}^{vac}) \rangle \quad (7)$$

where E_{Pt+ads}^{liq} is the DFT-calculated energy of the Pt surface plus adsorbate under explicit solvent, E_{Pt+ads}^{vac} is the DFT-calculated energy of the Pt surface plus adsorbate under vacuum, E_{Pt}^{liq} is the DFT-calculated energy of the clean Pt surface (without the adsorbate) under explicit solvent, E_{Pt}^{vac} is the DFT-calculated energy of the clean Pt surface under vacuum, and the bracket notation indicates the ensemble average. E_{Pt+ads}^{liq} are calculated as follows.[27] An initial guess of the conformation of the adsorbate is obtained by relaxing the structure of the adsorbate on a Pt(111) surface under I_h ice in DFT, according to the procedure in Section 2.4. The resulting Pt + adsorbate structure is then simulated under explicit solvent in MD in the NVT ensemble, following the procedures described in Sections 2.1 and 2.2. Positions of the solvent molecules are sampled at constant time intervals of at least 300 ps in order to generate at least five configurations of solvent molecules around the adsorbate. The conformations of the

DOI: 10.1021/acs.jcim.9b00089
J. Chem. Inf. Model. 2019, 59, 2190−2198

adsorbate and the surrounding solvent molecules are then rerelaxed in DFT following one of the strategies discussed in Section 2.4. E^{liq}_{Pt+ads} are the energies of the resulting conformations. E^{vac}_{Pt+ads} and E^{liq}_{Pt} are calculated by removing the solvent molecules (E^{vac}_{Pt+ads}) or adsorbate (E^{liq}_{Pt}) and recalculating the system energy in DFT. These calculations are "single point" calculations, where all atoms are held fixed. Values of ΔE^{DFT}_{int} are reported as averages taken over at least five configurations of solvent molecules.

2.3.2. Implicit Solvation. ΔF^{imp}_{sol} are calculated as

$$\Delta F^{imp}_{sol} = (F^{imp}_{Pt+ads} - E^{vac}_{Pt+ads}) - (F^{imp}_{Pt} - E^{vac}_{Pt}) \quad (8)$$

where F^{imp}_{Pt+ads} and F^{imp}_{Pt} are free energies (electronic energies plus free energies of solvation) of the Pt surface with the adsorbate and the clean Pt surface, respectively, calculated under implicit solvation, and E^{vac}_{Pt+ads} and E^{vac}_{Pt} are the electronic energies of same systems calculated under vacuum (i.e., with implicit solvation turned off). Values of F^{imp} are calculated in DFT using the VASPsol method.[19] VASPsol adds a dielectric term to the Hamiltonian that simulates a solvent continuum. The dielectric constant is set to 78.40 for pure water and 54.39 for the 50/50 H_2O/CH_3OH mixed solvent.[54] Technically, free energies calculated in this way are Gibbs free energies (i.e., G^{imp}_{Pt+ads} and G^{imp}_{Pt}); however, since $P\Delta V$ is expected to be 2 orders of magnitude smaller than ΔE for these systems,[52] we use values calculated in this way to approximate the Helmholtz free energies (ΔF^{imp}_{sol}) in order to compare with ΔF^{MSS}_{sol}.

2.4. DFT Calculations. DFT calculations are performed with the Vienna Ab initio Simulation Package (VASP),[55−58] which uses periodic boundary conditions and plane-wave basis sets. The Perdew, Burke, and Ernzerhof (PBE)[59] variation of the generalized gradient approximation (GGA) is used for electron exchange and correlation, and the projector augmented wave (PAW)[60,61] method is used to calculate interactions between the valence and core electrons to an energy cutoff of 400 eV. Gaussian smearing with a smearing factor of 0.1 eV is used for all calculations. The D2 method is employed to improve modeling of dispersion.[62] The effect of the dispersion model on ΔE_{int} is discussed in the Supporting Information. The first Brillouin zone is sampled with $7 \times 7 \times 1$ Monkhorst−Pack[63] k-point meshes. Electronic structures are calculated self-consistently and considered to be converged when the difference in the electronic energy between subsequent iterations falls below 10^{-5} eV.

Conformations of adsorbates and in some cases the surrounding solvent molecules are obtained using partial geometry relaxations performed with the quasi-Newton algorithm. The partial relaxations are carried out as follows. In relaxations carried out under vacuum, implicit solvation, and I_h ice, adsorbate atoms are allowed to relax, while all other atoms are held fixed. In relaxations carried out under explicit solvent, the adsorbate and the solvent molecules that are hydrogen bonded to it are allowed to relax, while all other atoms are held fixed. In all partial geometry relaxations, geometries are considered to be converged when the forces on all of the nonfixed atoms fall below 0.03 eV/Å. The Pt atoms are held fixed in all DFT simulations. This choice has a minor influence on the adsorbate binding energies and structures (see Supporting Information).

2.5. Hydrogen Bond Criteria. Hydrogen bonds (HBs) are identified using geometric criteria as follows.[64] The distance between the solvent oxygen atom and the electronegative atom on the adsorbate (i.e., the $O_{solvent}-N_{ads}/O_{ads}$ distance) must be ≤3.5 Å. Additionally, when the solvent molecule is a HB donor, the angle between the electronegative atom on the adsorbate, the solvent molecule oxygen atom, and the participating solvent molecule hydrogen atom (i.e., the $N_{ads}/O_{ads}-O_{solvent}-H_{solvent}$ angle) must be ≤30°, and the distance between the electronegative atom on the adsorbate and the participating hydrogen atom on the solvent molecule (i.e., the $N_{ads}/O_{ads}-H_{solvent}$ distance) must be ≤2.5 Å. When the solvent molecule is a HB acceptor, the angle between the solvent molecule oxygen atom, the electronegative atom on the adsorbate, and the participating hydrogen atom on the solvent molecule (i.e., the $O_{solvent}-N_{ads}/O_{ads}-H_{ads}$ angle) must be ≤30°, and the distance between the solvent molecule oxygen atom and the hydrogen atom on the adsorbate (i.e., the $O_{solvent}-H_{ads}$ distance) must be ≤2.5 Å. Hydrogen bonds can be formed between the adsorbates and solvent H_2O molecules as well as between adsorbates and solvent CH_3OH molecules when the mixed solvent is employed.

2.6. Rotational Dynamics of Solvent Molecules. The mobilities of the H_2O molecules that are hydrogen bonded to the adsorbates are studied using the dipole−dipole time correlation function (TCF).[65,66] The dipole−dipole TCF indicates how fast a H_2O molecule rotates away from its initial orientation after forming a hydrogen bond with the adsorbate. It is calculated as

$$C_\mu(t) = \frac{\langle \mu_i(t)\cdot\mu_i(0)\rangle}{\langle \mu_i(0)\cdot\mu_i(0)\rangle} \quad (9)$$

where $\mu_i(t)$ and $\mu_i(0)$ are the unit dipole vectors of the i^{th} hydrogen-bonded H_2O molecule at time $t = t$ and $t = 0$, respectively, and the bracket notation indicates an ensemble average. The vectors μ_i are obtained from the production runs of NVT MD simulations, which are carried out for 45 ns, where the first 5 ns are used for system equilibration, the last 40 ns are used for configurational sampling, and configurations are sampled every 100 fs during the production runs.

3. RESULTS

3.1. Free Energies of Solvation Calculated with Multiscale Sampling versus Implicit Solvation. Free energies of solvation calculated with multiscale sampling (ΔF^{MSS}_{sol}) and implicit solvation (ΔF^{imp}_{sol}) are listed in Table 1. Calculated ΔF_{sol} are all exothermic. In pure H_2O solvent, values of ΔF^{MSS}_{sol} follow the trend $C_3H_7O_3$* < COH* < CH_2OH* < NH_2* < NH* < CO*, with ΔF^{MSS}_{sol} for $C_3H_7O_3$* being quite appreciable at −0.91 eV and ΔF^{MSS}_{sol} for CO* being ∼0. Values of ΔF^{imp}_{sol} follow a similar trend as ΔF^{MSS}_{sol}. While $\Delta F^{MSS}_{sol} \approx \Delta F^{imp}_{sol}$ for the NH*, NH_2*, and CO* adsorbates, ΔF^{MSS}_{sol} and ΔF^{imp}_{sol} for the COH*, CH_2OH*, and $C_3H_7O_3$* adsorbates are different by 0.38, 0.12, and 0.56 eV, respectively. These differences could have energetic origins, entropic origins, or both, and we investigate these possibilities in Sections 3.2 and 3.3.

3.2. Energetic Origins. One reason for the differences between ΔF^{MSS}_{sol} and ΔF^{imp}_{sol} for some adsorbates could be that those adsorbates interact more strongly with H_2O than is captured by implicit solvation. Calculated interaction energies for the NH*, NH_2*, CO*, COH*, CH_2OH*, and $C_3H_7O_3$* adsorbates are listed in Table 1. Calculated ΔE_{int} are all negative, indicating favorable interactions with solvent. In general, the strengths of the interaction energies are related to the propensities of the adsorbates to form hydrogen bonds.

DOI: 10.1021/acs.jcim.9b00089
J. Chem. Inf. Model. 2019, 59, 2190−2198

Table 1. Solvation Free Energies (ΔF_{sol}), Interaction Energies (ΔE_{int}), and Interaction Entropies ($T\Delta S_{int}$) for NH*, NH_2*, CO*, COH*, CH_2OH*, $C_3H_7O_3$* Adsorbates on Pt(111) under Pure H_2O Solvent and a 50% H_2O/50% CH_3OH (w/w) Mixed Solvent at T = 300 K, Calculated with Multiscale Sampling (MSS), DFT with Explicit Solvation (DFT), DFT with Implicit Solvation (imp), and Molecular Dynamics (MD)[a]

	NH*	NH_2*	CO*	COH*	CH_2OH*	$C_3H_7O_3$*
			H_2O			
ΔF_{sol}^{MSS}	−0.20	−0.28	−0.02	−0.69	−0.30	−0.91
ΔF_{sol}^{imp}	−0.19	−0.26	−0.04	−0.31	−0.18	−0.35
ΔE_{int}^{DFT}	−0.34	−0.49	−0.09	−0.99	−0.63	−1.52
ΔE_{int}^{DFT}(mb)	−0.30	−0.46	−0.07	−0.63	−0.63	−1.33
$-T\Delta S_{int}^{MD}$	0.14	0.21	0.07	0.30	0.33	0.61
$-T\Delta S_{int}^{MD}$ (pert)	dnc	dnc	dnc	0.41	0.40	0.95
			50% H_2O/50% CH_3OH (w/w)			
ΔF_{sol}^{MSS}	−0.14	−0.16	0.04	−0.59	−0.14	−0.52
ΔF_{sol}^{imp}	−0.18	−0.24	−0.04	−0.29	−0.17	−0.31
ΔE_{int}^{DFT}	−0.30	−0.40	−0.03	−0.90	−0.46	−1.16
$-T\Delta S_{int}^{MD}$	0.16	0.24	0.07	0.31	0.33	0.64

[a]All values are calculated according to the procedures in Section 2 of this Article, except for those labeled "mb", which are calculated according to the procedure in Section 3.2, and those labeled "pert", which are discussed in Section 3.3. All values are in units of eV. dnc stands for "did not calculate".

Thus, NH*, NH_2*, COH*, CH_2OH*, and $C_3H_7O_3$*, which all feature either −NH or −OH groups, exhibit strong ΔE_{int}, whereas CO* exhibits ΔE_{int} < 0.1 eV. Snapshots of the NH*, NH_2*, COH*, CH_2OH*, and $C_3H_7O_3$* adsorbates along with representative configurations of hydrogen bonded H_2O molecules are shown in Figure 1.

If an adsorbate interacts more strongly with a H_2O molecule than is captured by implicit solvation, it could be because the adsorbate is forming a chemical bond with H_2O. To explore this possibility, we recalculated ΔE_{int}^{DFT}, this time only allowing the solvent molecules that are hydrogen bonded to the adsorbate to relax (and thus holding all other atoms, including those in the adsorbate, fixed). Calculations performed in this manner are labeled "mb" (for "method b") in Table 1 and Figure 1. We postulated that if the differences between ΔF_{sol}^{MSS} and ΔF_{sol}^{imp} were due to a chemical bond, that holding the adsorbate molecule fixed would prevent optimization of the chemical bond and thus result in a weaker (less negative) value of ΔE_{int}^{DFT}, which would result in a less exothermic value for ΔF_{sol}^{MSS}. ΔE_{int}^{DFT} calculated using this second relaxation method are tabulated in Table 1. Comparing these values with the original values of ΔE_{int}^{DFT}, the NH*, NH_2*, CO*, and CH_2OH* adsorbates show minor changes of 0.04 eV or less, while the COH* and $C_3H_7O_3$* adsorbates show much more significant differences of 0.36 and 0.19 eV, respectively. Note that for COH*, this difference is nearly identical to the difference between ΔF_{sol}^{MSS} and ΔF_{sol}^{imp}. Comparing the geometries of the COH*−H_2O and $C_3H_7O_3$*−H_2O systems calculated using the two different relaxation methods (i.e., comparing Figure 1c with Figure 1d and Figure 1g with Figure 1h), there are noticeable differences in the adsorbate−H_2O distances due the relaxation method used, lending credence to the hypothesis that these adsorbates form chemical bonds with H_2O solvent. In contrast, the relaxation method has at most a minor influence on the adsorbate−H_2O distance for NH*, NH_2*, and CH_2OH*.

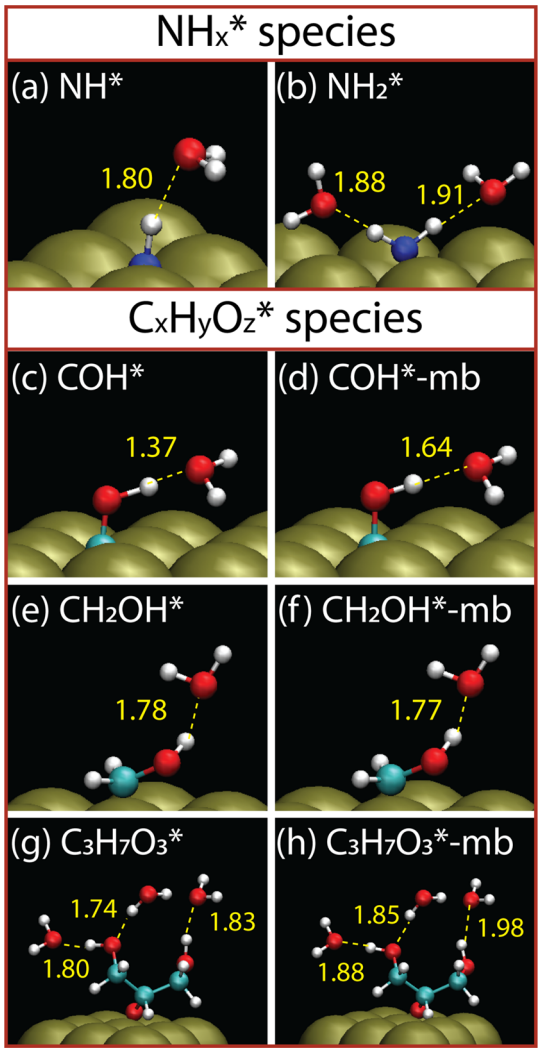

Figure 1. Representative geometries of NH* (a), NH_2* (b), COH* (c,d), CH_2OH* (e,f), and $C_3H_7O_3$* (g,h) adsorbates along with hydrogen-bonded H_2O molecules. For clarity, H_2O molecules that are not hydrogen bonded to the adsorbates are not rendered. All geometries were calculated according to the procedures in Section 2, except for those labeled "mb", which were calculated according to the procedure in Section 3.2. Color key: N = blue, H = white, O = red, C = cyan, Pt = gold. Distances are labeled in Å.

To further investigate the possibility of chemical bonds forming between the COH* and $C_3H_7O_3$* adsorbates and H_2O, we calculated the charge density differences for these adsorbates due to interaction with H_2O molecules (details about these simulations are provided in the Supporting Information). The results (Figure 2) show a significant increase in charge density between the COH* adsorbate and the H_2O molecule, suggesting formation of a chemical bond, whereas the charge density increase between the $C_3H_7O_3$* adsorbate and H_2O solvent is minor. Thus, we conclude that the COH* adsorbate forms a chemical bond with H_2O solvent, which results in a much more exothermic free energy of solvation when calculated with explicit solvent than with implicit solvent.

The differences between ΔF_{sol}^{MSS} and ΔF_{sol}^{imp} for CH_2OH* and $C_3H_7O_3$* must have different, or at least other, origins.

DOI: 10.1021/acs.jcim.9b00089
J. Chem. Inf. Model. 2019, 59, 2190−2198

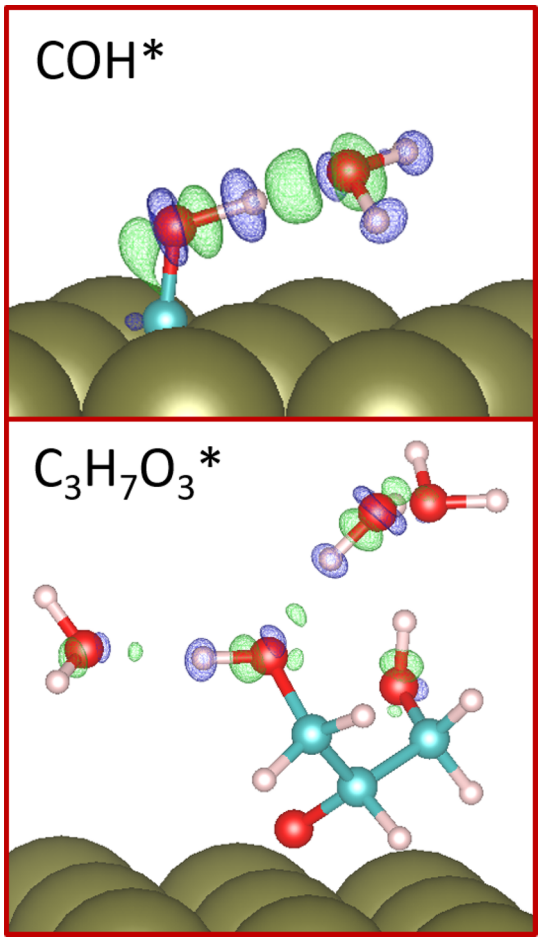

Figure 2. Charge density differences due to interaction for COH*–H_2O (top) and $C_3H_7O_3$*–H_2O (bottom). Color key: H = white, O = red, C = cyan, Pt = gold. Green and purple iso-surfaces represent regions of charge accumulation and depletion, respectively, and are rendered at values of 0.006 e/Å^3.

Another possibility is the interaction between the polar solvent and these polarizable adsorbates. To explore this possibility, we modified the polarity of the solvent by switching from a pure H_2O solvent (dielectric constant = 78.40) to a solution that is 50% H_2O/50% CH_3OH by weight (dielectric constant = 54.39). We reasoned that reducing the polarity of the solvent would reduce the strength of the adsorbate–solvent interaction for polarizable adsorbates and thus reduce the difference between ΔF_{sol}^{MSS} and ΔF_{sol}^{imp}. Values of ΔF_{sol}^{MSS} and ΔF_{sol}^{imp} calculated in mixed solvent are listed in Table 1. Values of ΔF_{sol}^{MSS} are more positive in the mixed solvent than in pure H_2O, with the most significant differences being for CH_2OH* (0.16 eV) and $C_3H_7O_3$* (0.39 eV). In fact, ΔF_{sol}^{MSS} and ΔF_{sol}^{imp} for CH_2OH* are nearly equal under the mixed solvent, suggesting the interaction between the polar solvent and this polarizable adsorbate as a reason for the difference between ΔF_{sol}^{MSS} and ΔF_{sol}^{imp} for CH_2OH* under pure H_2O.

For the $C_3H_7O_3$* adsorbate, the difference between ΔF_{sol}^{MSS} and ΔF_{sol}^{imp} in pure H_2O solvent of 0.56 eV seems to be due to a combination of chemical bonding and solvent polarity/adsorbate polarizability. To test this, we calculated ΔE_{int}^{DFT} for $C_3H_7O_3$* under the mixed solvent using the "mb" strategy discussed above. ΔE_{int}^{DFT} calculated in this manner is −1.05 eV, compared with the value of −1.16 eV calculated using the "standard" method (discussed in Section 2). This difference of 0.11 eV accounts for part of the difference of 0.21 eV between ΔF_{sol}^{MSS} and ΔF_{sol}^{imp} for $C_3H_7O_3$* in the mixed solvent, suggesting that chemical bonding indeed contributes to the differences between ΔF_{sol}^{MSS} and ΔF_{sol}^{imp}. Further, the much less significant difference between ΔF_{sol}^{MSS} and ΔF_{sol}^{imp} in the mixed solvent versus pure H_2O suggests that solvent polarity/adsorbate polarizability contributes as well.

3.3. Entropic Origins. Entropic contributions could also influence differences between ΔF_{sol}^{MSS} and ΔF_{sol}^{imp}, and we explore those in this section. Values of $-T\Delta S_{int}^{MD}$ are listed in Table 1. Values of $-T\Delta S_{int}^{MD}$ are all positive (i.e., $T\Delta S_{int}^{MD}$ are all negative), and thus they counteract values of ΔE_{int} in the calculation of ΔF_{sol}. Values of $-T\Delta S_{int}^{MD}$ follow the trend $C_3H_7O_3$* > CH_2OH* > COH* > NH_2* > NH* > CO*, which, other than that the order of COH* and CH_2OH* is reversed, is identical to the rank orders of ΔF_{sol}^{MSS} and ΔE_{int}^{DFT}. Thus, adsorbates that demonstrate strong interaction energies also exhibit large and negative interaction entropies. It is thus possible that the interaction entropies of adsorbates that exhibit chemical bonding and/or strong hydrogen bonds with highly polar solvents contribute to the differences between ΔF_{sol}^{MSS} and ΔF_{sol}^{imp}, and we investigate each of those effects separately here.

Unfortunately, the MSS method in its present form cannot capture the influence of chemical bonding on ΔS_{int}^{MD} since the classical force fields that are employed do not capture chemical bonding. Thus, we investigated how ΔS_{int}^{MD} would change if the bond between H_2O and the COH*, CH_2OH*, and $C_3H_7O_3$* adsorbates were stronger by manually perturbing the LJ cross terms for these interactions until the ΔE_{int}^{MD} for these adsorbates were almost equal to their ΔE_{int}^{DFT}. More details about these perturbations are provided in the Supporting Information. Values for $-T\Delta S_{int}^{MD}$ calculated in this way are labeled "pert" (for perturbed) in Table 1. Values of $-T\Delta S_{int}^{MD}$ for the COH* and CH_2OH* adsorbates increase by <0.10 eV when the force fields are altered in this way. The values of 0.10 eV or less are small and likely within the error caused by making a manual perturbation to the force field. Thus, entropy likely does not contribute to the differences between ΔF_{sol}^{MSS} and ΔF_{sol}^{imp} for these adsorbates. For the $C_3H_7O_3$* adsorbate, $-T\Delta S_{int}^{MD}$ increases by 0.34 eV when its interaction with H_2O is strengthened in the MD simulations. While this exact value should be taken lightly, given the rough manner in which it was obtained, its magnitude suggests that entropy cannot be ruled out as contributing to the difference between ΔF_{sol}^{MSS} and ΔF_{sol}^{imp} for $C_3H_7O_3$* in pure H_2O solvent.

Looking into the influence of polarity on ΔS_{int}, values of $-T\Delta S_{int}^{MD}$ calculated in pure H_2O are nearly identical to those calculated in mixed solvent, suggesting that the solvent polarity has little effect on ΔS_{int}. Hence, we conclude that differences between ΔF_{sol}^{MSS} and ΔF_{sol}^{imp} uncovered in this work are due to energetic effects caused by chemical bonding and/or strong hydrogen bonds induced by highly polar solvents, and, in the case of $C_3H_7O_3$*, entropic influences resulting from such interactions.

4. DISCUSSION

To this point, we have shown that the strengths of the adsorbate–solvent interactions are dominated by hydrogen bonding, interactions between a polar solvent and a polarizable adsorbate, and, in some cases, chemical bonding. Adsorbates that demonstrate strong ΔE_{int} with solvent also exhibit large, negative values of $T\Delta S_{int}^{MD}$. Because of this, values of ΔE_{int}^{DFT} are

DOI: 10.1021/acs.jcim.9b00089
J. Chem. Inf. Model. 2019, 59, 2190–2198

significantly compensated when calculating ΔF_{sol}^{MSS}. Here, we postulate that the large, negative values for $T\Delta S_{int}^{MD}$ are due to restricted dynamics of solvent molecules that interact strongly with catalytic surface adsorbates. To demonstrate this, we calculate dipole−dipole TCFs ($C_\mu(t)$), which illustrate the rotational dynamics of the solvent molecules that hydrogen bond to the adsorbates, along with their mean square displacements, which illustrate their translational dynamics, under pure H_2O solvent. The dipole−dipole TCF results are shown in Figure 3. The mean square displacements have

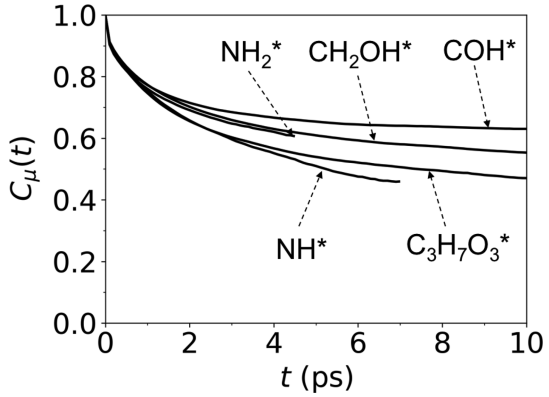

Figure 3. Dipole−dipole time correlation function as a function of time elapsed over the lifetime of a hydrogen bond for the NH*, NH_2*, COH*, CH_2OH*, and $C_3H_7O_3$* adsorbates.

similar trends as those of the dipole−dipole TCFs (see Supporting Information). On the graphs in Figure 3, the abscissae denote the time elapsed over the lifetime of a hydrogen bond. Once the hydrogen bond between the H_2O molecule and the adsorbate is broken, it is no longer counted toward $C_\mu(t)$. Thus, $C_\mu(t)$ values level off as t gets larger, and the different curve lengths are because the different adsorbates have different HB lifetimes. (More information about HB lifetimes is provided in the Supporting Information.) The $C_\mu(t)$ curves illustrate how the orientations of the dipole vectors of the H_2O molecules that are hydrogen bonded to the adsorbates change over time. At $t = 0$, $C_\mu(t) = 1$, and this value decreases as t increases, indicating rotation of the H_2O molecule. As t gets large, the H_2O molecule rotates enough that the geometric angle criteria for hydrogen bonding (see Section 2.6) are violated. When this happens, the $C_\mu(t)$ curves in Figure 3 end. When the H_2O molecules have more restricted rotational motions, their values of $C_\mu(t)$ are larger (i.e., they stay closer to 1). Thus, hydrogen-bonded H_2O molecules have less rotational mobility around adsorbates with $C_\mu(t)$ closer to 1. $C_\mu(t)$ calculated for the different adsorbates follow the trend COH* > CH_2OH* > NH_2* > $C_3H_7O_3$* > NH*. This suggests that H_2O molecules that are hydrogen bonded to COH* have the slowest rotational dynamics, whereas H_2O molecules that are hydrogen bonded to NH* have the fastest. The trend for $C_\mu(t)$ is similar to that for ΔE_{int}, except for $C_3H_7O_3$*, where the H_2O molecules exhibit fast rotational dynamics; however, this adsorbate has multiple −OH groups that contribute to ΔE_{int}^{DFT}, so the relationship between $C_\mu(t)$ and ΔE_{int}^{DFT} will be different than for the other adsorbates. The translational dynamics of the hydrogen-bonded water molecules (shown in the Supporting Information) follow a similar trend. Taken together, these results suggest that strong interactions between catalytic adsorbates and solvent molecules restrict the rotational and translational dynamics of the solvent molecules. As entropy is related to mobility, we argue that the loss of the rotational and translational mobilities of the solvent molecules contribute to the large $T\Delta S_{int}^{MD}$ exhibited by adsorbates that interact strongly with solvent.

5. CONCLUSIONS

In this work, we used a combination of DFT and classical MD to explore the free energies of solvation for catalytic surface adsorbates under H_2O and mixed H_2O/CH_3OH solvents, and we additionally identified the origins of the energetic and entropic contributions to the free energies of solvation. We found that the free energies of solvation have large contributions from both the adsorbate−solvent interaction energies as well as their entropies. Adsorbate−solvent interaction energies are dominated by hydrogen bonding, solvent polarity/adsorbate polarizability, and, in some cases, chemical bonding. Adsorbates that exhibit strong interactions with solvent molecules restrict the rotational dynamics of those solvent molecules, and this influences the adsorbate−solvent interaction *entropies* as well. Thus, the interaction energies are largely compensated by the interaction entropies when calculating the free energies of solvation. That said, the free energies of solvation can be rather significant, with values in this work being as large as −0.91 eV. Implicit solvation using the VASPsol method can be used to calculate free energies of solvation for catalytic adsorbates that do not interact chemically with solvent molecules and that do not demonstrate enhanced interactions with highly polar solvents. For adsorbates that do exhibit chemical bonds or strong interactions with polar solvents, we present a multiscale sampling method for calculating the free energies of solvation. While this method is powerful, it has limitations. For one, it is computationally intensive, requiring the use of DFT and MD simulations and also sampling multiple configurations of solvent in DFT. Further, this method uses rigid catalytic surface adsorbates and Pt surfaces, and thus does not fully capture thermal effects (nor does implicit solvation). Our groups are presently working on methods to address both issues.

■ ASSOCIATED CONTENT

Supporting Information

The Supporting Information is available free of charge on the ACS Publications website at DOI: 10.1021/acs.jcim.9b00089.

Further details about simulations and adsorbate structures (PDF)

■ AUTHOR INFORMATION

Corresponding Author

*E-mail: rgetman@clemson.edu.

ORCID

Ryan S. DeFever: 0000-0001-5311-6718
Sapna Sarupria: 0000-0001-7692-8313
Rachel B. Getman: 0000-0003-0755-0534

Notes

The authors declare no competing financial interest.

■ ACKNOWLEDGMENTS

This research was funded by the National Science Foundation under grant numbers CBET-1554385 (Getman) and AGS-

DOI: 10.1021/acs.jcim.9b00089
J. Chem. Inf. Model. 2019, 59, 2190−2198

1541944 (Sarupria). Simulations were performed on the Palmetto Supercomputer Cluster, which is maintained by the Cyberinfrastructure Technology Integration Group at Clemson University. We thank Dr. Steven Louis Pellizzeri, who worked as a postdoctoral associate in our group, for helpful discussions about charge density analysis, and Anna Hardymon, who was an undergraduate intern in our group through the Clemson University EURKEA! program, for testing the influence of simulation box size on ΔE_{int}^{MD}.

REFERENCES

(1) Garcia-Rates, M.; López, N. Multigrid-Based Methodology for Implicit Solvation Models in Periodic DFT. *J. Chem. Theory Comput.* **2016**, *12*, 1331−1341.
(2) Yeh, K.-Y.; Wasileski, S. A.; Janik, M. J. Electronic Structure Models of Oxygen Adsorption at the Solvated, Electrified Pt (111) Interface. *Phys. Chem. Chem. Phys.* **2009**, *11*, 10108−10117.
(3) Sha, Y.; Yu, T. H.; Liu, Y.; Merinov, B. V.; Goddard, W. A., III Theoretical Study of Solvent Effects on the Platinum-Catalyzed Oxygen Reduction Reaction. *J. Phys. Chem. Lett.* **2010**, *1*, 856−861.
(4) Keith, J. A.; Muñoz-García, A. B.; Lessio, M.; Carter, E. A. Cluster Models for Studying CO_2 Reduction on Semiconductor Photoelectrodes. *Top. Catal.* **2015**, *58*, 46−56.
(5) Iyemperumal, S. K.; Deskins, N. A. Evaluating Solvent Effects at the Aqueous/Pt (111) Interface. *ChemPhysChem* **2017**, *18*, 2171−2190.
(6) Faheem, M.; Suthirakun, S.; Heyden, A. New Implicit Solvation Scheme for Solid Surfaces. *J. Phys. Chem. C* **2012**, *116*, 22458−22462.
(7) Faheem, M.; Heyden, A. Hybrid Quantum Mechanics/Molecular Mechanics Solvation Scheme for Computing Free Energies of Reactions at Metal-Water Interfaces. *J. Chem. Theory Comput.* **2014**, *10*, 3354−3368.
(8) Faheem, M.; Saleheen, M.; Lu, J.; Heyden, A. Ethylene Glycol Reforming on Pt (111): First-Principles Microkinetic Modeling in Vapor and Aqueous Phases. *Catal. Sci. Technol.* **2016**, *6*, 8242−8256.
(9) Behtash, S.; Lu, J.; Walker, E.; Mamun, O.; Heyden, A. Solvent Effects in the Liquid Phase Hydrodeoxygenation of Methyl Propionate over a Pd (111) Catalyst Model. *J. Catal.* **2016**, *333*, 171−183.
(10) Behtash, S.; Lu, J.; Mamun, O.; Williams, C. T.; Monnier, J. R.; Heyden, A. Solvation Effects in the Hydrodeoxygenation of Propanoic Acid over a Model Pd (211) Catalyst. *J. Phys. Chem. C* **2016**, *120*, 2724−2736.
(11) Saleheen, M.; Heyden, A. Liquid-Phase Modeling in Heterogeneous Catalysis. *ACS Catal.* **2018**, *8*, 2188−2194.
(12) Getman, R. B.; Xu, Y.; Schneider, W. F. Thermodynamics of Environment-Dependent Oxygen Chemisorption on Pt(111). *J. Phys. Chem. C* **2008**, *112*, 9559−9572.
(13) Gokhale, A. A.; Kandoi, S.; Greeley, J. P.; Mavrikakis, M.; Dumesic, J. A. Molecular-Level Descriptions of Surface Chemistry in Kinetic Models using Density Functional Theory. *Chem. Eng. Sci.* **2004**, *59*, 4679−4691.
(14) Dumesic, J. A. *The Microkinetics of Heterogeneous Catalysis*; An American Chemical Society Publication, 1993.
(15) Rogal, J.; Reuter, K. *Ab Initio Atomistic Thermodynamics for Surfaces*; A Primer; 2006.
(16) Campbell, C. T.; Sellers, J. R. The Entropies of Adsorbed Molecules. *J. Am. Chem. Soc.* **2012**, *134*, 18109−18115.
(17) Jones, T. E.; Rocha, T. C.; Knop-Gericke, A.; Stampfl, C.; Schlögl, R.; Piccinin, S. Thermodynamic and Spectroscopic Properties of Oxygen on Silver under an Oxygen Atmosphere. *Phys. Chem. Chem. Phys.* **2015**, *17*, 9288−9312.
(18) Soon, A.; Todorova, M.; Delley, B.; Stampfl, C. Oxygen Adsorption and Stability of Surface Oxides on Cu (111): A First-Principles Investigation. *Phys. Rev. B: Condens. Matter Mater. Phys.* **2006**, *73*, 165424.
(19) Mathew, K.; Sundararaman, R.; Letchworth-Weaver, K.; Arias, T.; Hennig, R. G. Implicit Solvation Model for Density-Functional Study of Nanocrystal Surfaces and Reaction Pathways. *J. Chem. Phys.* **2014**, *140*, 084106.
(20) Hartnig, C.; Spohr, E. The Role of Water in the Initial Steps of Methanol Oxidation on Pt (111). *Chem. Phys.* **2005**, *319*, 185−191.
(21) Nørskov, J. K.; Rossmeisl, J.; Logadottir, A.; Lindqvist, L.; Kitchin, J. R.; Bligaard, T.; Jonsson, H. Origin of the Overpotential for Oxygen Reduction at a Fuel-Cell Cathode. *J. Phys. Chem. B* **2004**, *108*, 17886−17892.
(22) Huang, Z.-Q.; Long, B.; Chang, C.-R. A Theoretical Study on the Catalytic Role of Water in Methanol Steam Reforming on PdZn (111). *Catal. Sci. Technol.* **2015**, *5*, 2935−2944.
(23) Dix, S. T.; Scott, J. K.; Getman, R. B.; Campbell, C. T. Using Degrees of Rate Control to Improve Selective n-Butane Oxidation over Model MOF-Encapsulated Catalysts: Sterically-Constrained Ag_3 Pd (111). *Faraday Discuss.* **2016**, *188*, 21−38.
(24) Jinnouchi, R.; Kodama, K.; Morimoto, Y. DFT Calculations on H, OH and O Adsorbate Formations on Pt (111) and Pt (332) Electrodes. *J. Electroanal. Chem.* **2014**, *716*, 31−44.
(25) Michel, C.; Zaffran, J.; Ruppert, A. M.; Matras-Michalska, J.; Jedrzejczyk, M.; Grams, J.; Sautet, P. Role of Water in Metal Catalyst Performance for Ketone Hydrogenation: A Joint Experimental and Theoretical Study on Levulinic Acid Conversion into gamma-Valerolactone. *Chem. Commun.* **2014**, *50*, 12450−12453.
(26) Neurock, M.; Wasileski, S. A.; Mei, D. From First Principles to Catalytic Performance: Tracking Molecular Transformations. *Chem. Eng. Sci.* **2004**, *59*, 4703−4714.
(27) Bodenschatz, C. J.; Sarupria, S.; Getman, R. B. Molecular-Level Details about Liquid H_2 OInteractions with CO and Sugar Alcohol Adsorbates on Pt(111) Calculated using Density Functional Theory and Molecular Dynamics. *J. Phys. Chem. C* **2015**, *119*, 13642−13651.
(28) Nie, X.; Luo, W.; Janik, M. J.; Asthagiri, A. Reaction Mechanisms of CO_2 Electrochemical Reduction on Cu (111) Determined with Density Functional Theory. *J. Catal.* **2014**, *312*, 108−122.
(29) Santana, J. A.; Mateo, J. J.; Ishikawa, Y. Electrochemical Hydrogen Oxidation on Pt (110): A Combined Direct Molecular Dynamics/Density Functional Theory Study. *J. Phys. Chem. C* **2010**, *114*, 4995−5002.
(30) Saavedra, J.; Doan, H. A.; Pursell, C. J.; Grabow, L. C.; Chandler, B. D. The Critical Role of Water at the Gold-Titania Interface in Catalytic CO Oxidation. *Science* **2014**, *345*, 1599−1602.
(31) Xie, T.; Bodenschatz, C. J.; Getman, R. B. Insights into the Roles of Water on the Aqueous Phase Reforming of Glycerol. *React. Chem. Eng.* **2019**, *4*, 383.
(32) Bodenschatz, C. J.; Zhang, X.; Xie, T.; Arvay, J.; Sarupria, S.; Getman, R. B. Multiscale Sampling of a Heterogeneous Water/Metal Catalyst Interface using Density Functional Theory and Force-Field Molecular Dynamics. *JoVE* **2019**, in press.
(33) Xie, T.; Sarupria, S.; Getman, R. B. A DFT and MD Study of Aqueous-Phase Dehydrogenation of Glycerol on Pt (111): Comparing Chemical Accuracy Versus Computational Expense in Different Methods for Calculating Aqueous-Phase System Energies. *Mol. Simul.* **2017**, *43*, 370−378.
(34) Kyriakou, V.; Garagounis, I.; Vasileiou, E.; Vourros, A.; Stoukides, M. Progress in the Electrochemical Synthesis of Ammonia. *Catal. Today* **2017**, *286*, 2−13.
(35) Golberg, A.; Sack, M.; Teissie, J.; Pataro, G.; Pliquett, U.; Saulis, G.; Stefan, T.; Miklavcic, D.; Vorobiev, E.; Frey, W. Energy-Efficient Biomass Processing with Pulsed Electric Fields for Bioeconomy and Sustainable Development. *Biotechnol. Biofuels* **2016**, *9*, 94.
(36) Greeley, J.; Mavrikakis, M. Competitive Paths for Methanol Decomposition on Pt (111). *J. Am. Chem. Soc.* **2004**, *126*, 3910−3919.
(37) Offermans, W.; Jansen, A.; Van Santen, R. Ammonia Activation on Platinum {111}: A Density Functional Theory Study. *Surf. Sci.* **2006**, *600*, 1714−1734.
(38) Plimpton, S. Fast Parallel Algorithms for Short-Range Molecular Dynamics. *J. Comput. Phys.* **1995**, *117*, 1−19.

DOI: 10.1021/acs.jcim.9b00089
J. Chem. Inf. Model. 2019, 59, 2190−2198

(39) Bussi, G.; Donadio, D.; Parrinello, M. Canonical Sampling Through Velocity Rescaling. *J. Chem. Phys.* **2007**, *126*, 014101.
(40) Nosé, S. A Molecular Dynamics Method for Simulations in the Canonical Ensemble. *Mol. Phys.* **1984**, *52*, 255−268.
(41) Hoover, W. G. Canonical Dynamics: Equilibrium Phase-Space Distributions. *Phys. Rev. A: At., Mol., Opt. Phys.* **1985**, *31*, 1695.
(42) MacKerell, A. D., Jr; Bashford, D.; Bellott, M.; Dunbrack, R. L., Jr; Evanseck, J. D.; Field, M. J.; Fischer, S.; Gao, J.; Guo, H.; Ha, S.; Joseph-McCarthy, D.; Kuchnir, L.; Kuczera, K.; Lau, F. T. K.; Mattos, C.; Michnick, S.; Ngo, T.; Nguyen, D. T.; Prodhom, B.; Reiher, W. E.; Roux, B.; Schlenkrich, M.; Smith, J. C.; Stote, R.; Straub, J.; Watanabe, M.; Wirkiewicz-Kuczera, J.; Yin, D.; Karplus, M. All-Atom Empirical Potential for Molecular Modeling and Dynamics Studies of Proteins. *J. Phys. Chem. B* **1998**, *102*, 3586−3616.
(43) Jorgensen, W. L.; Jenson, C. Temperature Dependence of TIP3P, SPC, and TIP4P Water from NPT Monte Carlo Simulations: Seeking Temperatures of Maximum Density. *J. Comput. Chem.* **1998**, *19*, 1179−1186.
(44) Jorgensen, W. L.; Chandrasekhar, J.; Madura, J. D.; Impey, R. W.; Klein, M. L. Comparison of Simple Potential Functions for Simulating Liquid Water. *J. Chem. Phys.* **1983**, *79*, 926−935.
(45) Jorgensen, W. L.; Maxwell, D. S.; Tirado-Rives, J. Development and Testing of the OPLS All-Atom Force Field on Conformational Energetics and Properties of Organic Liquids. *J. Am. Chem. Soc.* **1996**, *118*, 11225−11236.
(46) Rappé, A. K.; Casewit, C. J.; Colwell, K.; Goddard, W. A., III; Skiff, W. UFF, A Full Periodic Table Force Field for Molecular Mechanics and Molecular Dynamics Simulations. *J. Am. Chem. Soc.* **1992**, *114*, 10024−10035.
(47) Lorentz, H. Ueber die Anwendung des Satzes vom Virial in der Kinetischen Theorie der Gase. *Ann. Phys.* **1881**, *248*, 127−136.
(48) Berthelot, D. Sur le Mélange des Gaz. *C. r. hebd. séances Acad. Sci.* **1898**, *126*, 1703−1855.
(49) Manz, T. A.; Limas, N. G. Introducing DDEC6 Atomic Population Analysis: Part 1. Charge Partitioning Theory and Methodology. *RSC Adv.* **2016**, *6*, 47771−47801.
(50) Hockney, R. W.; Eastwood, J. W. *Computer Simulation Using Particles*; CRC Press, 1988.
(51) Shirts, M. R.; Pande, V. S. Solvation Free Energies of Amino Acid Side Chain Analogs for Common Molecular Mechanics Water Models. *J. Chem. Phys.* **2005**, *122*, 134508.
(52) van der Vegt, N. F.; van Gunsteren, W. F. Entropic Contributions in Cosolvent Binding to Hydrophobic Solutes in Water. *J. Phys. Chem. B* **2004**, *108*, 1056−1064.
(53) Yu, H.-A.; Karplus, M. A Thermodynamic Analysis of Solvation. *J. Chem. Phys.* **1988**, *89*, 2366−2379.
(54) Akerlof, G. Dielectric Constants of Some Organic Solvent-Water Mixtures at Various Temperatures. *J. Am. Chem. Soc.* **1932**, *54*, 4125−4139.
(55) Kresse, G.; Hafner, J. Ab Initio Molecular Dynamics for Liquid Metals. *Phys. Rev. B: Condens. Matter Mater. Phys.* **1993**, *47*, 558.
(56) Kresse, G.; Hafner, J. Ab Initio Molecular-Dynamics Simulation of the Liquid-Metal−Amorphous-Semiconductor Transition in Germanium. *Phys. Rev. B: Condens. Matter Mater. Phys.* **1994**, *49*, 14251.
(57) Kresse, G.; Furthmüller, J. Efficiency of Ab-Initio Total Energy Calculations for Metals and Semiconductors using a Plane-Wave Basis Set. *Comput. Mater. Sci.* **1996**, *6*, 15−50.
(58) Kresse, G.; Furthmüller, J. Efficient Iterative Schemes for Ab Initio Total-Energy Calculations using a Plane-Wave Basis Set. *Phys. Rev. B: Condens. Matter Mater. Phys.* **1996**, *54*, 11169.
(59) Perdew, J. P.; Burke, K.; Ernzerhof, M. Generalized Gradient Approximation Made Simple. *Phys. Rev. Lett.* **1996**, *77*, 3865.
(60) Blöchl, P. E. Projector Augmented-Wave Method. *Phys. Rev. B: Condens. Matter Mater. Phys.* **1994**, *50*, 17953.
(61) Kresse, G.; Joubert, D. From Ultrasoft Pseudopotentials to the Projector Augmented-Wave Method. *Phys. Rev. B: Condens. Matter Mater. Phys.* **1999**, *59*, 1758.
(62) Grimme, S. Semiempirical GGA-Type Density Functional Constructed with a Long-Range Dispersion Correction. *J. Comput. Chem.* **2006**, *27*, 1787−1799.
(63) Monkhorst, H. J.; Pack, J. D. Special Points for Brillouin-Zone Integrations. *Phys. Rev. B* **1976**, *13*, 5188.
(64) Luzar, A.; Chandler, D. Hydrogen-Bond Kinetics in Liquid Water. *Nature* **1996**, *379*, 55.
(65) Pal, S.; Chakraborty, K.; Khatua, P.; Bandyopadhyay, S. Microscopic Dynamics of Water around Unfolded Structures of Barstar at Room Temperature. *J. Chem. Phys.* **2015**, *142*, 055102.
(66) Zhang, X.; Sewell, T. E.; Glatz, B.; Sarupria, S.; Getman, R. B. On the Water Structure at Hydrophobic Interfaces and the Roles of Water on Transition-Metal Catalyzed Reactions: A Short Review. *Catal. Today* **2017**, *285*, 57−64.

DOI: 10.1021/acs.jcim.9b00089
J. Chem. Inf. Model. 2019, 59, 2190−2198